Appl. Phys. A 70, 39–45 (2000) / Digital Object Identifier (DOI) 10.1007/s003399900128

Applied Physics A
Materials
Science & Processing

Photoluminescence in $GdVO_4$:Bi^{3+}, Eu^{3+} red phosphor

B.N. Mahalley[1], **S.J. Dhoble**[2], **R.B. Pode**[1], **G. Alexander**[3]

[1] Department of Physics, Nagpur University, Nagpur 440 010, India
[2] Kamla Nehru College, Nagpur 440 009, India
[3] Rare Earth Development Section, Bhabha Atomic Research Centre, Mumbai 400 085, India

Received: 2 November 1998/Accepted: 22 June 1999/Published online: 3 December 1999

Abstract. The doubly doped (Bi^{3+} and Eu^{3+}) $GdVO_4$ powder is synthesized by hydrolyzed colloid reaction (HCR) technique and formation of material is confirmed by XRD measurement. Surface morphology has been studied by SEM measurement and the result shows uniform surface morphology. The average particle size observed by SEM is about 1 μm. The Fritsch particle sizer is used to study the particle size distribution. It distributes from O.15 to 3.57 μm. The small particle size (less than 5 μm) and the narrow particle size distribution, are the necessary requirements of good phosphor material. Photoluminescence result shows a narrow emission line of Eu^{3+} ion (4 nm FWHM) at 618 nm. The Eu^{3+} emission intensity is enhanced by a factor of five with the addition of small amount of Bi^{3+}. The emission bands of VO_4^{3-} and Bi^{3+} partially overlap with the excitation band of Eu^{3+}. The process of energy transfer from Bi^{3+} to Eu^{3+} is discussed here. The energy transfer probability is strongly dependent upon the Bi^{3+} and Eu^{3+} concentrations, with a maximum for 0.2 mol % of Bi^{3+} and 3 mol % of Eu^{3+}. It drastically decreases for higher concentrations. For photoluminescent applications, the quantum efficiency (QE) of a phosphor material is an important parameter. The QE of $GdVO_4$:Bi, Eu(0.2, 3) is 76%. The $GdVO_4$:Bi, Eu(0.2, 3) material is proposed as an efficient photoluminescent phosphor.

PACS: 78.55

The luminescent materials are widely used in present-day life. Their best-known applications, are in cathode-ray tubes and fluorescent lamps. The efficient phosphors are applied in the X-ray intensifying screens, cathode-ray tubes, and fluorescent lamps. The two groups of luminescent materials can be distinguished: the phosphors with lattice excitation and the ones with direct excitation in the activator ions. The X-ray and CRT phosphors belong to the first category and a lot of them are used in both applications. In all the phosphors applied in fluorescent lamps, the exciting UV radiation is directly absorbed by the activator ions and no delocalized states are involved in the luminescence process.

In the last two decades, the development of new phosphors for lighting and other applications has centered on the refractory host matrices, (hexa-aluminate and yttrium oxide) activated with trivalent rare earths. The introduction of rare earths has resulted in a drastic improvement of the performance of luminescent devices based on these phosphors. The blue, green, red, and other phosphors are available in the market.

The trivalent europium-doped vanadates have attracted a great deal of interest for use as a red phosphor in colour television, cathode-ray tubes, and in fluorescent lamps [1]. The first red-emitting rare-earth phosphor YVO_4:Eu^{3+}, was introduced by Levine and Palilla [2] as a red primary in colour television in 1964. In single-crystal form, it was used as an excellent polarizer and laser material [3]. $GdVO_4$:Tm, Ho and $GdVO_4$:Nd crystals with diode laser as an excitation source are used for the development of lasers [4, 5]. $GdVO_4$:Bi powder has been proposed as a possible scintillating material in computer tomography [6]. They have attractive and important applications in different field. For these applications, however, homogeneous, high-quality, oxygen-deficiency-free vanadates are required. It is a well-known fact that the vanadium penta-oxide vaporizes readily above its melting point at 690 °C, causing incongruent changes in both the vanadium and oxygen stoichiometries [7–9]. In several cases, the oxygen deficiency can create problems in the optical application of YVO_4 [9].

The different methods available to produce oxygen deficiency-free rare earth vanadate are (i) the special flux technique [10]; (ii) the hydrothermal reaction technique [11]; and (iii) low-temperature (< 100 °C) aqueous-solution technique. The wet techniques are strongly recommended for synthesis of high-quality phosphors in powder form, required in high-resolution displays and miniature CRTs [12]. The high temperature solid-state-reaction techniques produce relatively large grain-size materials, in addition to oxygen-defect colour centres. The reduction of particle size by mechanical grinding, results in crystal particle damage and lower luminescent efficiency. The solid-state-reaction technique, therefore, is not recommended for synthesis of powder phosphors. Necessary requirements of good phosphor powders

are: (a) a fine particle size (< 5 μm); (b) a narrow particle-size distribution; (c) a large surface area; (d) high purity and homogeneity; and (e) an efficient energy transfer (electronic transition) from the sensitizer to an activator ion, if any.

Pure YVO_4, in aqueous solution, was first synthesized by the reaction of yttrium nitrate and ammonium metavanadate by Arbit and Serbrennikov in 1965 [13]. Krylov et al. patented this technique for industrial applications [14]. In subsequent years, many workers prepared yttrium vanadates by aqueous solution with different starting materials and patented the techniques [15–18]. Recently, a hydrolyzed colloidal-type mixtures of the aqueous $V_2O_5 + Y_2O_3 + H_2O$ system has been used for preparation of YVO_4 powder [19]. Very fine particles of powder material, synthesized by this method, were observed and this is one of the requirements of the good phosphor.

In the present investigation, $GdVO_4$:Eu^{3+} and $GdVO_4$:Bi^{3+}, Eu^{3+} powders were prepared by hydrolyzed colloid reaction (HCR) technique. The formation of crystalline powder was checked by XRD measurement. The SEM technique was used to study the surface morphology. Particle size and surface area were also measured. Luminescence properties of Eu^{3+} ion and energy transfer between Bi^{3+} to Eu^{3+} in $GdVO_4$ powder are reported.

1 Experimental

For preparing doped $GdVO_4$ powder material, Gd_2O_3, Eu_2O_3 (Indian Rare Earth Ltd. and 99.9% pure), spectra pure V_2O_5, and Bi_2O_3 powders were used as starting materials. The HCR method and subsequent calcining at higher temperature were used to synthesize the doped $GdVO_4$ powder. Constituent powders Gd_2O_3, V_2O_5, and a small amount of dopant ions were dry-mixed thoroughly by mechanical crushing for 1 h and then transferred to 100 ml of double-distilled water. This solution was placed in a polyethylene beaker for mixing. For production of colloidal mixture, the mixing was carried out for a sufficient time period at room temperature in the air using a magnetic stirrer. The glass needle (the iron needle inside the glass) was used as a grinding medium. It is known that the acidification of an aqueous system of $V_2O_5 + Gd_2O_3 + H_2O$ plays an important role in the formation of complex colloids [19] and therefore, the pH behaviour of this mixture was investigated first. Figure 1 shows the changes in pH with the mixing time at room temperature. It initially decreases, later on starts increasing, and finally stabilizes to 6.9. Before the mixing started, the colour of the aqueous mixture was dark yellow and pH was found to be 4.9. As the mixing continued, the colour changed to orange-yellow after 10 h due to the formation of tri-metavanadate ($Gd_2V_3O_9{\cdot}xH_2O$) and had pH = 3.8. After 30 h of mixing, it became red-brown, forming the deca-vanadate intermediate phase $Gd_2V_{10}O_{10}{\cdot}25H_2O$ with pH = 6.5. The aqueous mixture became white after 50 h of mixing due to the formation of gadolinium vanadate and had pH = 6.9. The temperature of the aqueous mixture changed from 25 °C to 35 °C during the course of mixing. The formation of tri-metavanadate and deca-vanadate were confirmed by XRD measurements. The white aqueous mixture, obtained after 50 h of mixing, was filtered to get white wet powder. This powder was dried at

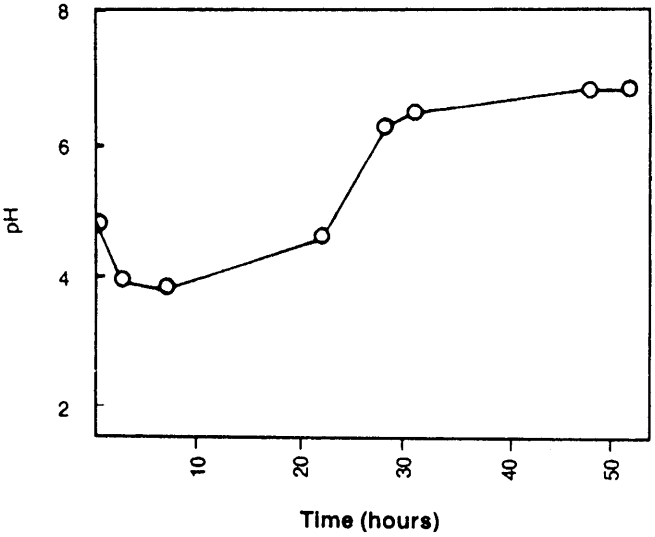

Fig. 1. pH values in (Bi^{3+} + Eu^{3+})-doped $V_2O_5 + Gd_2O_3 + H_2O$ aqueous mixture after different mixing times at room temperature

100 °C for 15 min and then calcined at 750 °C for 24 h and at 1000 °C for 5 h in the air.

The formation of gadolinium vanadate powder was confirmed by studying the XRD pattern. The observed pattern matched with the standard data of the compound (JCPD File No. 17-260). Particle size and surface area were determined. The fluorescence spectra were recorded on a Jobin-Yvon spectroflurometer at room temperature.

2 Results and discussion

Formation of $GdVO_4$:Bi^{3+}, Eu^{3+} (0.2, 3 mol %) as synthesized powder material was confirmed by the XRD pattern. The Bi^{3+} (0.2 mol %) and Eu^{3+} (3 mol %) ions concentrations are in the starting material and not in the final synthesized powder. The rare earth vanadate has a tetragonal structure and is a system of linked oxygen tetrahedra having Gd and V atoms at their centres (Fig. 2). In this figure, circles represent Gd atoms [C] and V atoms are at the centres of small tetrahedra (A and B) whose corners show the positions of the oxygen atoms. V atoms are almost completely hidden within the tetrahedra of their surrounding oxygen atoms. The impurities Bi^{3+} or Eu^{3+} ions enter into a substitutional Gd^{3+} cation site. The [VO_4^{3-}–Bi^{3+}] structure is formed. The VO_4^{3-} group may be surrounded by more than one Bi^{3+} impurity ions.

2.1 Scanning electron microscopy (SEM)

Fine particle size, narrow particle-size distribution, and large surface area are the important requirements of good phosphor. These parameters were measured. The particle size was measured using scanning electron microscopy. The SEM microphotograph gives information about the particle size (grain size). Since the doped $GdVO_4$ powder is a good insulator, it was coated with gold to obtain an acceptable SEM picture. Figure 3 shows the SEM observation in $GdVO_4$:Bi^{3+}, Eu^{3+} powder. An uniform surface morphology was observed. Results show that the powder was agglomerated and the particle

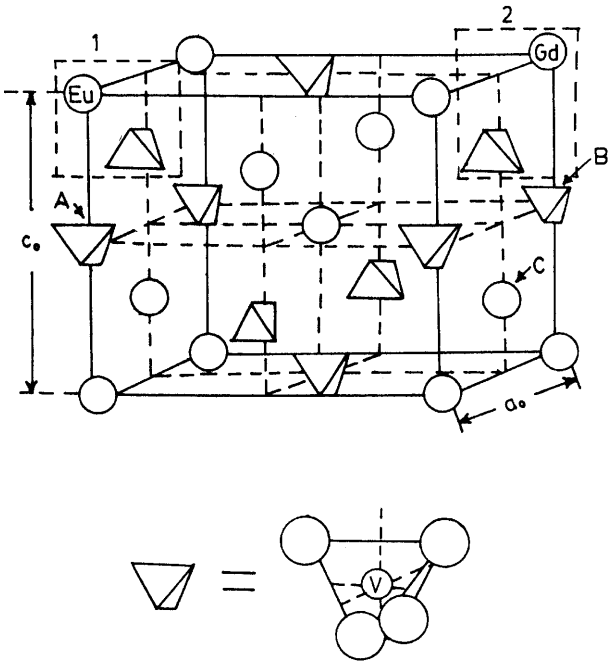

Fig. 2. The lattice positions in the tetragonal unit cell of doped $GdVO_4$. The Eu or Bi atoms are represented by *circles* and V atoms are at the centres of the *small tetrahedra* whose corners mark the positions of the oxygen atoms

size varies from 0.3 to 1.6 μm. Their average particle size was found to be about 1 μm. It seems that the observance of lower particle size much less than 5 μm in calcined powder is the peculiarity of the HCR technique, compared to other methods of preparation such as the solid-state diffusion technique and combustion process where large grains are observed. Further, the Fritsch particle sizer was used to get exact information about the particle-size distribution. The surface area was also measured.

The particle-size distribution of $GdVO_4$:Bi^{3+}, Eu^{3+} is shown in Fig. 4. The surface area was about 2.0245 ($\pm$0.0046) m^2/g. The particle size distribution, varies from 0.15 to 3.57 μm as shown in the figure. The average particle size is of the order 1.03 μm of 50 wt. % of $GdVO_4$:Bi, Eu. The narrow particle-size distribution and fine particles observed in our sample are necessary requirements of a good phosphor material and are in agreement with standard results as reported earlier [20].

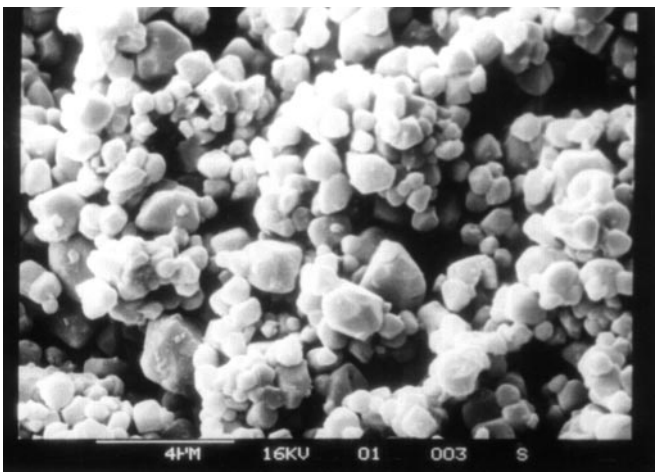

Fig. 3. SEM microphotograph of calcined white $GdVO_4$:Bi, Eu (0.2, 3) powder

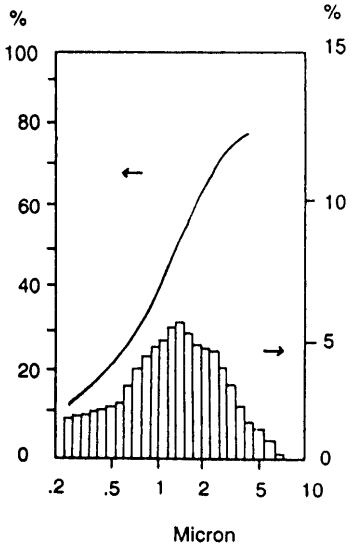

Fig. 4. Particle-size distribution of $GdVO_4$:Bi, Eu (0.2, 3) 50 wt. % average = 1.03 μm

2.2 Photoluminescence studies

In pure $GdVO_4$ powder, very weak emission lines of Dy^{3+} at 480 to 570 nm, Sm^{3+} at around 605 nm are found due to the presence of impurity ions in the starting Gd_2O_3 material. The broad and weak band of the VO_4^{3-} group at 450 nm were observed at room temperature, excited at 325 nm. These results are consistent with the earlier reported ones and hence not reproduced here [6]. Emission lines of Gd^{3+} ions include four sharp lines lying between 310 and 315 nm, and three weak lines at about 306 nm corresponding to the transitions $^6P_{7/2} \rightarrow {}^8S_{7/2}$ (310 to 315 nm) and $^6P_{5/2} \rightarrow {}^8S_{7/2}$ (306 nm), respectively, excited at 274 nm [21, 22]. Such emission lines of Gd^{3+} are not observed in our sample. The part of excitation energy absorbed by Gd^{3+} result in non-radiative emission. This energy may be utilised for excitation of Bi^{3+}, VO_4^{3-} group, or Eu^{3+} ions.

It is well known that Bi^{3+} can be used as an activator, as well as a sensitizer of luminescence. Many workers [23–28] have studied the luminescent properties of Bi^{3+} and energy transfer from Bi^{3+} to Bi^{3+} ion or to another activator in an oxide host lattice. The emission peak varies from the UV to the red region, depending on the host lattice [24]. Also, the energy transfer probability between Bi^{3+} ions or from Bi^{3+} ions to another activator varies widely with the host lattice [26, 27]. The excitation and emission spectra of $GdVO_4$:Bi^{3+} (1 mol %) show a band at 338 nm (curve a; monitored at 557 nm) and 557 nm (curve b; excited at 338 nm), respectively, along with a small shoulder at around 480 nm at room temperature, and are shown in Fig. 5. This shoulder at 480 nm may be due to the VO_4^{3-} group. With the introduction of Bi^{3+} into $GdVO_4$, the emission peaks move to a higher wavelength side by some amount [24, 28]. The impurity, emission lines, observed in pure $GdVO_4$ powder, were completely suppressed by the addition of Bi^{3+} impurity.

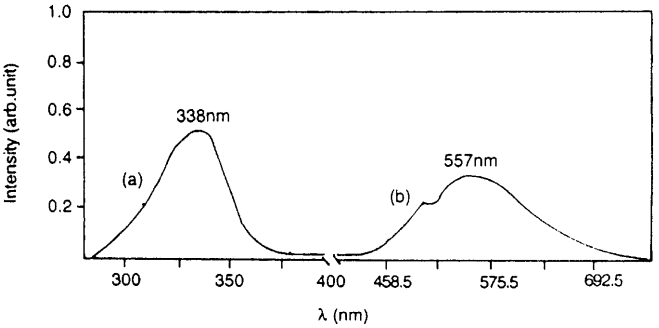

Fig. 5. Photoluminescence spectra of $GdVO_4$:Bi (1 mol %) powder. (a) Excitation spectrum, monitored at 557 nm. (b) Emission spectrum, excited at 338 nm

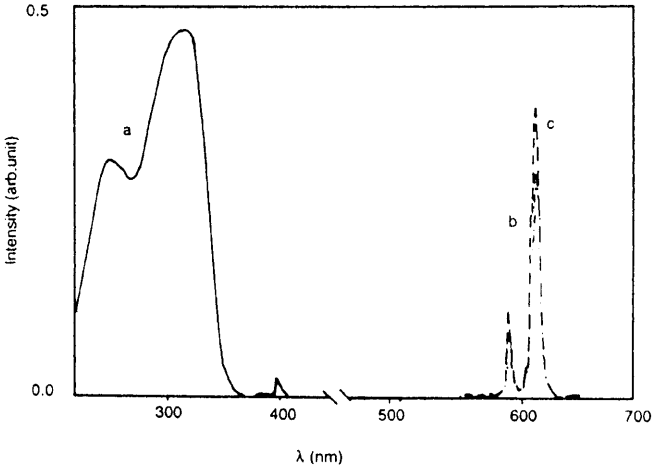

Fig. 6. Photoluminescence spectra of $GdVO_4$:Eu (3 mol %) powder. (a) Excitation curve, monitored at 618 nm. (b) Emission curve, excited at 254 nm. (c) Emission curve, excited at 328 nm

The broad excitation band at 338 is due to $^1S_0 \rightarrow {}^1P_1$ transition and the emission band 557 nm occurs due to $^3P_1 \rightarrow {}^1S_0$ transition. The ground state of a free Bi^{3+} ion with ns^2 configuration is the $^1S_0$ state. The excited states come from the $nsnp$ configuration and are $^3P_0$, $^3P_1$, $^3P_2$, and $^1P_1$ states in order of increasing energy [24, 29]. The excitation results from $^1S_0$ to $^1P_1$ transitions. If the cubic symmetry is perfect, the other transitions are completely forbidden [30]. When the excited state is relaxed to $^3P_1$ state, emission results due to the $^3P_1$ to $^1S_0$ transition. The earlier work on Bi^{3+} ion luminescence in an oxide host lattice showed that the excitation band corresponds to the $^1S_0 \rightarrow {}^1P_1$ transition and emission band to the $^3P_1 \rightarrow {}^1S_0$ transition [23]. Similar results have also been reported in silica-gel glass [27]. The emission of Bi^{3+} is more prominent than the intrinsic emission of pure $GdVO_4$.

Figure 6 shows the excitation (monitored at 618 nm) and emission bands (excited at 328 nm) in $GdVO_4$:Eu^{3+} (3 mol %). The excitation curve consists of prominent peaks at 254 and 328 nm along with shoulder at 400 nm. The 328-nm excitation wavelength is situated near the excitation wavelengths of pure $GdVO_4$ (325 nm) and $GdVO_4$:Bi^{3+} (338 nm). The intensity of the 254-nm line is lower compared to that of the 328-nm line. The fluorescence lamp is a low-pressure mercury discharge lamp with a layer of phosphor particles on the inside surface of a glass tube. The internal radiation generated is mostly at 254 nm (85%) which is the resonance wavelength of the mercury vapour discharge. The other 15% is distributed among 185, 315, 365, 430, 546, and 578.5 nm. The 328-nm excitation wavelength is the prominent one in our sample and hence was selected for excitation in $GdVO_4$:Eu^{3+}. The emission spectrum shows peaks at 596 and 618 nm (4 nm FWHM) due to $^5D_0 \rightarrow {}^7F_1$ and $^5D_0 \rightarrow {}^7F_2$ transitions, respectively (curve c in Fig. 6). The $^5D_0 \rightarrow {}^7F_2$ emission line of Eu^{3+} splits into two components at 615 and 618 nm due to lowering of local site symmetry of Eu^{3+} ions [31]. The Eu^{3+} emission curve of $GdVO_4$:Eu^{3+} (3 mol %), excited at 254 nm is also given for comparison (curve b). No change in emission curve is observed, except some change in peak intensities. These results are consistent with the earlier reported results [21, 32, 33].

To increase the luminescence output and to avoid the concentration quenching, a small amount of a co-activator (called sensitizer, S) is desirable. The co-activator ion efficiently absorbs the excitation energy and transfers it to the activator ion. Figure 7 shows the 618-nm Eu^{3+} (1 mol %) emission peak intensity variation with Bi^{3+} ion concentration in $GdVO_4$:Bi, Eu powder. The experimental photoluminescence intensity is plotted against the concentration. The results show that the Eu^{3+} emission intensity enhances sharply from 0.05 to 0.2 mol % of Bi^{3+} concentration. Maximum emission intensity is observed for 0.2 mol % of Bi^{3+} and then starts decreasing for higher concentration. The sensitization effect of Bi^{3+} ion on the Eu^{3+} emission ion varies with Bi^{3+} concentration. For higher concentration of Bi^{3+} ion, the Bi_n^{3+} aggregates may be formed (where $n > 1$). These aggregates act as trapping centres and dissipate absorbed energy non-radiatively, instead of transferring to Eu^{3+} activator ion. The energy transfer probability from Bi^{3+} to Eu^{3+} is strongly dependent on the Bi^{3+} ion concentration. Optimum energy transfer is observed for 0.2 mol % of Bi^{3+}. The energy transfer is not only depending on the sensitizer Bi^{3+} concentration, but also on the Eu^{3+} activator ion concentration. Figure 8 shows the dependence of energy transfer from Bi^{3+} to Eu^{3+} on the Eu^{3+} ion concentration. The experimental photoluminescence intensity is plotted against the Eu^{3+} ion concen-

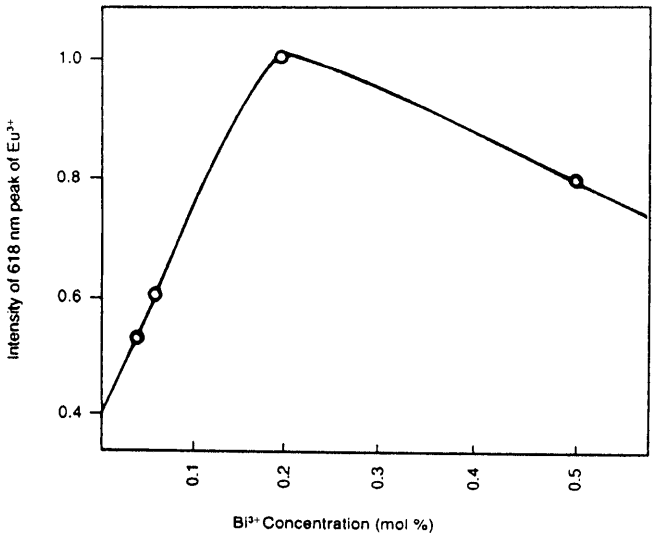

Fig. 7. The Eu^{3+} ion emission intensity (618 nm) variation with Bi^{3+} ion concentration. The Eu^{3+} ion concentration is kept constant to 1 mol %

tration. In doubly doped $GdVO_4$, the Bi^{3+} ion concentration was fixed to 0.2 mol % and Eu^{3+} ion concentration was varied from 0.01 to 3 mol %. The 618-nm Eu^{3+} emission line intensity enhances sharply in the region from 0.01 to 1 mol % of Eu^{3+}. It increases slowly in the region from 1 to 3 mol % and stabilizes for higher concentration. These results show that the optimum energy transfer is observed for 0.2 mol % of Bi^{3+} and 3 mol % of Eu^{3+} ion in $GdVO_4$ powder.

Figure 9 shows the photoluminescence spectrum of Bi^{3+} (0.2 mol %) + Eu^{3+} (3 mol %) in the $GdVO_4$ powder at room temperature, excited at 318 nm. The excitation curve of doubly doped vanadate contains prominent peaks at 254 and 318 nm, monitored at 618 nm. The 318-nm wavelength was used for excitation in our sample. This line is also in the excitation region of the pure $GdVO_4$ (325 nm), $GdVO_4$:Bi^{3+} (338 nm), and $GdVO_4$:Eu^{3+} (328 nm). Earlier, it was reported that the excitation spectrum of Eu^{3+} consists of peaks at 277, 368, 400, and 420 nm [27]. The 318-nm light excites VO_4^{3-} group, Bi^{3+}, and also Eu^{3+} ions. These ions may transfer their emitted energy to Eu^{3+} ion. A strong emission line of Eu^{3+} at 618 nm (4 nm FWHM) due to the $^5D_0 \rightarrow {}^7F_2$ transition was observed in double-doped vanadate along with a small peak at 596 nm due to the $^5D_0 \rightarrow {}^7F_1$ transition. The Eu^{3+} emission curve (curve c, Fig. 9), excited at 254 nm is also given for comparison. No change in emission curve is observed, except some small change in emission intensities of peaks of Eu^{3+}.

Results show that the Eu^{3+} ion emission intensity in the doubly doped $GdVO_4$ is enhanced by five times compared to $GdVO_4$:Eu^{3+} (3 mol %). The increase in intensity is attributed to the energy transfer from Bi^{3+} to Eu^{3+}. The 318-nm light excites VO_4^{3-} group, Bi^{3+}, and also Eu^{3+} ions. The emitted energy of VO_4^{3-} (450 nm), and Bi^{3+} (557 nm) ion transfers to Eu^{3+} ion, resulting in increase of Eu^{3+} ion emission intensity. Also, Bi^{3+} ion emission band overlaps Eu^{3+} $f - f$ transitions to $^5D_1$ level. The emission from $^5D_1$ level is not observed. The $^5D_1$ level may decay to $^5D_0$ level. The $^5D_0 \rightarrow {}^7F_0$ emission line of Eu^{3+} ion is at 578.2 nm. However, the overlapping of emissions of Bi^{3+} and VO_4^{3-} group,

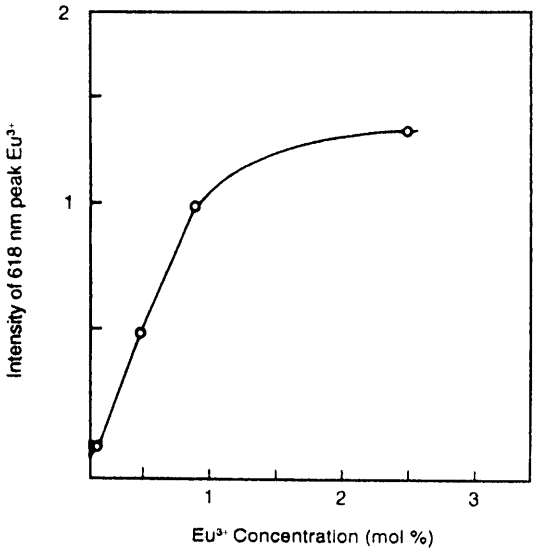

Fig. 8. The 618-nm emission peak intensity of Eu^{3+} ion variation with Eu^{3+} ion concentration. The Bi^{3+} ion concentration is fixed to 0.2 mol %

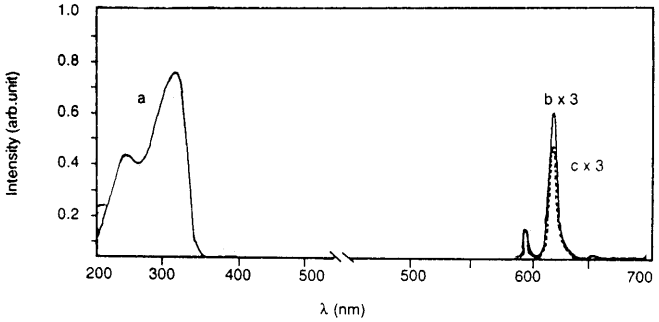

Fig. 9. Photoluminescence spectra of $GdVO_4$:Bi, Eu (0.2, 3) at room temperature. (a) Excitation curve, monitored at 618 nm. (b) Emission curve, excited at 318 nm. (c) Emission curve, excited at 254 nm

and excitation of Eu^{3+} ion was not prominent. The emitted photons of VO_4^{3-} group and Bi^{3+} ions may be reabsorbed partially by the activation of Eu^{3+} ion thereby enhancing red emission of Eu^{3+} ion by a factor of five. Further, the role of VO_4^{3-} group, in energy transfer may be confirmed by making low-temperature luminescence measurements. The part of excitation energy absorbed by Gd^{3+} ions, may emit non-radiatively. The emission lines of Gd^{3+} ions appear from 310 to 315 nm. The emitted energy may be reabsorbed and transfer to Eu^{3+} ion through the lattice in more than one step.

Table 1 gives the photoluminescence quantum efficiencies of some important red photoluminescent materials. For photoluminescent applications, the quantum efficiency (QE) of a phosphor is often regarded as a measure of its figure of merit. The term QE refers to the extent to which a phosphor can convert an absorbed UV photon into a visible photon on a one-to-one basis. The QE of our sample was measured on an experimental set-up at BARC, Bombay to an accuracy of ±2%. Results demonstrate that our sample prepared by HCR technique is at par with some of the samples reported by other worker (Table 1).

Results reported above may be explained as follows. The system of dopant ion in host lattice shows luminescence upon excitation. The dopant ion interacts with the surrounding ions. The environment of the dopant ion is not static; the surrounding ions vibrate about some average positions, so that the crystalline field varies. The emission energy is given by:

$$\Delta E_S = 2S\hbar\omega\,, \tag{1}$$

where S is a measure of interaction between dopant ion and the surrounding vibrating lattice. If the return from the excited state to the ground state is radiative, then the quantum yield is maximum. This is usually not the case. The relaxed excited state may, however, reach the crossing of the two parabolae (excited and ground states) if the temperature is high enough. It is possible to return to the ground state in a non-radiative manner. Most of the luminescence energy is then given up as heat to the lattice. If the luminescent centres come together, they may show interaction with each other resulting in a new phenomenon. The relaxed excited state of the sensitizer may transfer its energy to an activator ion. In a double-doped sample, the energy transfer probability between sensitizer and activator could be given, according to

Table 1. Quantum efficiencies QE of some red photoluminescence materials under ultraviolet excitation at room temperature

Material	Sample origin	Emission wavelength/ nm	Halfwidth/ nm	QE/ %	Ref.
$CaSiO_3$:Pb, Mn	—	615	94	85	1
$Cd(BO_2)_2$:Mn	—	618	75	78	1
YVO_4:Eu	—	620	4	89	1
Y_2O_3	—	619	3	92	1
YVO_4:Eu	Philips	Red	—	99	35
YVO_4:Eu	BARC	Red	—	99	35
Y_2O_3:Eu	Philips	Red	—	99	35
Gd_2O_3:Eu	BARC	Red	—	85	35
$Y_3Al_5O_{12}$:Eu^{3+}	BARC	Red	—	90	35
YVO_4:Eu	Derbi	Red	—	95	36
Y_2O_2S:Eu	Hitachi	Red	—	95	36
YVO_4:Eu	G. Blasse	Red	—	70	37
$GdVO_4$:Eu	Nag. Univ.	618	4	69(±2)	Present work
$GdVO_4$:Bi, Eu	Nag. Univ.	618	4	76(±2)	Present work

Dexter [34], as

$$P_{SA} = 2\frac{\pi}{h} |< SA^* \mid H_{SA} \mid S^*A |^2 \int g_S(E) g_A(E) dE \,, \qquad (2)$$

where the integral is the spectral overlap. H_{SA} is the interaction Hamiltonian and * indicates the excited state.

A high value of energy transfer probability from the sensitizer to an activator requires a considerable amount of (i) resonance, i.e. the sensitizer emission should overlap spectrally with the absorption band(s) of the activator ion, (ii) interaction, which may be of multipole–multipole type or of exchange type.

Two mechanisms, radiative and non-radiative, for energy transfer have been postulated [28]. The total energy transfer probability is proportional to the spectral overlap between emission of the sensitizer and absorption of the activator in both mechanisms. In radiative energy transfer, the energy transfer is through emission of the sensitizer and reabsorption by an activator and requires considerable overlap of the emission region of the sensitizer and absorption region of the activator. Non-radiative energy transfer is associated with the resonance between absorber and emitter and consists of several steps.

The increase in intensity of the 618-nm emission line of Eu^{3+} in $GdVO_4$:Bi, Eu (0.2, 3) could be explained as follows. The energy migration in Gd^{3+} based compounds open interesting possibilities to obtain new, efficient luminescent material. In the above powders, Bi^{3+}, VO_4^{3-} group, etc. absorb excitation energy and transfer their energy to the Eu^{3+} ions through the host lattice. Moreover, this part of the excitation energy absorbed by the Gd^{3+} ions may be transferred non-radiatively to Bi^{3+}, VO_4^{3-} group, and subsequently to Eu^{3+} ions. The energy transfer should not be restricted to one step, so that we expect that the first transfer step is followed by many others. Emission bands of Bi^{3+} (557 nm) and VO_4^{3-} (450 nm) were observed in gadolinium-based samples. Appearance of these bands may partially take part in the energy migration to Eu^{3+} ions. The radiation probability of the host gadolinium ions should be negligible. For a Bi^{3+} concentration larger than 0.2 mol %, the distance between Bi^{3+} ions would be small. Aggregates of these ions are formed, which act as energy traps. The energy transfer from Bi^{3+} to Bi^{3+} ions may be more efficient than that from Bi^{3+} to Eu^{3+} ions. The excitation reaches a site where it is lost non-radiatively. The luminescence efficiency of such composition will be low. Significant reduction in energy transfer from the sensitizer Bi^{3+} to the activator Eu^{3+} ions is observed.

3 Conclusion

From the results presented and discussed here, the $GdVO_4$:Bi, Eu (0.2, 3) material is the suitable red phosphor. The surface morphology is uniform. The particle size distributes in the narrow region from 0.15 to 3.57 μm and the average particle size was about 1.03 μm for 50 wt. %. The surface area is 2.0245(±0.0046) m^2/g. These are the essential requirements of good phosphor material. There is a partial energy transfer between Bi^{3+} to Eu^{3+}, resulting in an increase of Eu^{3+} red emission intensity by five times. The energy transfer probability is strongly dependent on the sensitizer Bi^{3+} concentration. For higher concentrations of Bi^{3+} (more than 0.2 mol %), $Bi^{3+} \rightarrow Bi^{3+}$ energy transfer is efficient. This results in concentration quenching of Eu^{3+} emission. The $GdVO_4$:Bi, Eu (0.2, 3) powder could be used as an efficient red phosphor.

Acknowledgements. The authors are thankful to the Director, Jawarharlal Nehru Aluminium Research Design and Development Centre, Nagpur for providing surface area and particle-size distribution measurement facilities.

References

1. R.C. Ropp: *Luminescence and the Solid State* (Elsevier, Amsterdam 1991) p. 330
2. A.K. Levine, F.C. Palilla: Appl. Phys. Lett. **5**, 118 (1964)
3. R.A. Fields, M.Birnbaum, C.L. Fincher: Appl. Phys. Lett. **51**, 1885 (1987)
4. P.J. Morris, W. Luty, H.P. Weber, Y.D. Zavartsev, P.A. Studenikin, I. Shcherbakov, A.I. Zagumenyi: Opt. Commun. (Netherlands) **111**, 493 (1994)
5. P.K. Mukhopadhyay, J. George, S.K. Sharma, R. Kapoor, D.D. Bhawalkar: National Laser Symposium, CAT, Indore (India) 49 (6–8 Feb. 1997)
6. G. Leppart, S. Peudenier, E. Bayer, B.C. Grabmaier, G. Blasse: Appl. Phys. A **59**, 69 (1994)

7. S. Killingbeck: Ph.D. Thesis, University of Kansas, Lawrence, USA (1963)
8. S. Eradi, F.W. Ainger: J. Cryst. Growth **128**, 1025 (1993)
9. S. Eradi, F.W. Ainger: Mater. Res. Soc. Proc. **329**, 245 (Pittsburgh, 1994)
10. S. Eradi: J. Cryst. Growth **134**, 1 (1993)
11. A.A. Fotoev, B.V. Schulgin, A.S. Moskvin, F.F. Gabrilov: *Vandievye Kristallofosfory* (Uralskij Nauchnji Centre, Askad, Nauk SSR, Nauka, Moscow (1976) (in Russian)
12. Performance Improvement of Miniature Cathode Ray Tubes AAMRL-82-062 (April 1988)
13. E.A. Arbit, V.V. Serebrennikov: Russ. J. Inorg. Chem. **10**, 220 (1965)
14. V.S. Krylov, I.N. Popkov, R.L. Magunov, M.M. Puring, K.H.S. Bagdasarov, R.F. Zhagina, V.I. Popov: US Patent 3667901 (1972)
15. V.I. Popov, K.H.S. Bagdasarov, I.N. Buseva, M.V. Mokhosoev: Sov. Phys. Cryst. **13**, 974 (1969)
16. R.C. Ropp: US Patent 3580861 (1971)
17. R.C. Ropp, R. Oakley: German Patent 2056172 (1971)
18. R.C. Ropp, B. Carroll: J. Inorg. Nucl. Chem. **39**, 1303 (1977)
19. S. Eradi: J. Mat. Sci. **30**, 4950 (1995)
20. N.A. Dhas, K.C. Patil: J. Mater. Chem. **4**(3), 491 (1994)
21. S. Tie, Q. Su, Y. Yu: Phys. Status Solidi A **147**, 267 (1995)
22. C. Parent, P. Bochu, A. Daoudi, G. Le Flem: J. Solid State. Chem. **43**, 190 (1982)
23. A.C. van Der Steen, J.J.A. van Hesteren, A.P. Slok: J. Electrochem. Soc. **128**, 1327 (1981)
24. G. Blasse, A. Bril: J. Chem. Phys. **48**, 217 (1968)
25. F. Kellendonk, T. van den Belt, G. Blasse: J. Chem. Phys. **76**, 114 (1982)
26. G. Blasse, A. Bril: J. Chem. Phys. **47**, 1920 (1967)
27. M. Wang, X. Fan, G. Xiong: J. Phys. Chem. Solids **56**, 859 (1995)
28. R.B. Pode, S.J. Dhoble: Phys. Status Solidi B **203**, 571 (1997)
29. A. Fukuda: Sci. Light (Japan) **13**, 64 (1964)
30. F. Seitz: J. Chem. Phys. **6**, 150 (1938)
31. X. Fan, M. Wang, Y. Yu, Q. Wu: J. Phys. Chem. Solids **57**, 1259 (1996)
32. A. Daoudi, G. Le Flem: J. Solid State Chem. **43**, 190 (1982)
33. D. Meib, S. Kemmler-Sack: Mat. Chem. Phys. **35**, 114 (1993)
34. D.L. Dexter: J. Chem. Phys. **21**, 836 (1953)
35. BARC News Letter, ed. by M.R. Balkrishanan, Library & Information Division, BARC, Mumbai (India) No. 153, 7 (1996)
36. G. Alexander, P. Ramkrishna, T.K. Mukherjee: Ind. J. Pure Appl. Phys. **31**, 531 (1993)
37. G. Blasse: *Radiationless Processes*, ed. by B. Di Bartolo (Plenum Press, New York 1980) p. 287